Current Nanoscience, 2021, *17*, 139-150

RESEARCH ARTICLE

Bioconjugation of Bacteriophage Pf1 and Extension to Pf1-Based Bionanomaterials

Taylor Urquhart[1], Bradley Howie[1], Lei Zhang[1], Kam Tong Leung[1] and John F. Honek[1,*]

[1]*Department of Chemistry and Waterloo Institute for Nanotechnology, Faculty of Science, University of Waterloo, Waterloo, ON, Canada*

ARTICLE HISTORY

Received: November 14, 2019
Revised: December 27, 2019
Accepted: May 21, 2020

DOI:
10.2174/1573413716999200614142202

Abstract: ***Background*:** Filamentous bacteriophages such as M13 are an important class of macromolecular assembly, rich in chemical moieties that can be used to impart modifiable positions at the nanoscale.

***Objective*:** To explore the structurally more complex Pf1 bacteriophage with respect to a diverse set of bioconjugation reactions and to prepare novel fluorescently-labelled Pf1-based composite biomembranes for future applications in areas such as nanoporous filtration biofilms and photoconducting nanocomposite materials.

***Methods*:** Pf1 was characterized with respect to amine (N-terminal, Gly1 and Lys20), carboxylate (aspartate, glutamate), and aromatic (tyrosine) modification and its extension to the creation of functional biomaterials. Modification with an amine reactive fluorophore was carried out with Pf1.

***Results*:** The reaction profiles between M13 and Pf1 differ, with M13 capable of modification at two primary amines on its major coat protein, while Pf1 is capable of a single reaction per coat protein. Subsequent to the production of dye-functionalized Pf1, a biocomposite of wild type and functionalized Pf1 could be fabricated into a bulk material by glutaraldehyde (amine-reactive) crosslinking. These biomaterials were characterized by scanning electron and confocal microscopy, showing a distribution of patches of functionalized Pf1 within the main Pf1 construct.

***Conclusion*:** The current study provides a framework for future fabrication of advanced bionanomaterials based on the Pf1 bacteriophage.

Keywords: Bacteriophage, Pf1, TAMRA, crosslinking, bioconjugation, electron microscopy.

1. INTRODUCTION

Biomolecules present an important category of well-defined architectures from which order and features in the nanoscale can be derived. Viruses [1, 2], capsule proteins [3, 4], liposomes [5, 6], DNA [7] as well as other derived biological structures such as nanocellulose [8] well-represent the diversity of scaffolds employed to fabricate novel bionanomaterials. From a nanodimensional building block perspective, viruses are a host-dependent replicating entity which can be produced in high yields with excellent monodispersity and are rich in reactive moieties specific to the amino acid composition of their viral coat proteins. Hence viruses are currently of great interest as complex but highly controllable scaffolds for various applications [9-14].

M13 is a filamentous virus which has a considerable impact in areas such as medicine [15-19], nanomaterial synthesis [20-24], energy [25-29], biosensor fabrication [30-36] and functional materials [37-40]. Pf1, a more complex and larger filamentous virus, has not been explored in terms of application and bioconjugate capabilities; though it is used as a nuclear magnetic resonance (NMR) co-solvent to align DNA and proteins in a magnetic field [41, 42]. The fabrication of novel Pf1-based biomaterials, such as chromophore-labelled biofilms and porous membranes, as well as conductive Pf1 composites, would be important components in future advanced monitorable gas/water separation processes and conductive photoactivated materials. The greater length and complexity of Pf1 should allow for more intricate scaffold architectures in these advanced materials than previously available. In order to enable these strategies however, fundamental knowledge is required on the reactions and crosslinking properties of this bacteriophage.

Filamentous bacteriophages (viruses which infect bacteria) are classified based on their mode of infection as well as their capsid structures. The F-specific filamentous phages (Ff) infect their host bacterium by adhering to the pilus of F+ strains. The representative of the Ff phages are two separate structural classifications, class I and class II, of which M13 and Pf1 belong respectively [43]. M13 utilizes *Escherichia coli* as its host organism and Pf1 requires *Pseudomonas ae-*

*Address correspondence to this author at the Department of Chemistry and Waterloo Institute for Nanotechnology, Faculty of Science, University of Waterloo, 200 University Avenue West, Waterloo, ON, Canada, N2L 3G1; Tel/Fax: 01-1-519-888-4567 x35817; E-mail: jhonek@uwaterloo.ca

1875-6786/21 $65.00+.00

ruginosa. Both are composed of a single-stranded DNA (ssDNA) genome encapsulated by many copies of a small, and alpha-helical major coat protein, and several copies of minor coat proteins at their tips.

For M13, the major coat protein ($p8_{M13}$) is present in 2700 copies and for Pf1, the major coat protein ($p8_{Pf1}$) is present in 7400 copies. Additionally, M13 has approximate dimensions of 7 x 900 nm and Pf1 of 6 x 2000 nm [44]. Well-characterized strategies to functionalize M13 including genetic, chemical modification of canonical amino acids and bioorthogonal reactions have enabled the extensive application of this phage [45-47]. Since the major coat proteins $p8_{M13}$ (A_1EGDDPAK_8AA FNSLQASATE YIGYAWAMVV VIVGATIGIK LFKKFTSKAS) and $p8_{Pf1}$ (G_1VIDTSAVES AITDGQGDMK$_{20}$ AIGGYIVGAL VILAVAGLIY SMLRKA) differ in amino acid composition, the bioconjugation toolbox available to the two is expected to differ.

Early work on Pf1 exploring the structure of the viral coat yielded data on the reactivity of several of the amino acid residues of $p8_{Pf1}$ [48]. This study showed very preliminary chemical modification information in order to understand amino acid residues that were solvent exposed related to viral coat structure. It reported that Tyr25, N-terminal Gly1, Lys20, and Asp4 were exposed to the reaction. With respect to reactive amines that form stable conjugates, M13 is capable of modification at the N-terminus and Lys8 [49], while preliminary work with Pf1 utilizing succinic anhydride suggested that the N-terminus and Lys20 (though less reactive than Gly1) were exposed [48]. No other research has been reported on further exploring the reactivity of solvent-exposed $p8_{Pf1}$ amine-containing residues.

If Pf1 is only capable of N-terminal modification, reaction with this phage may yield a larger but simpler and more uniform bioconjugate than M13 with a much greater number of subunits in the viral sheath, allowing for additional bioconjugation and crosslinking reactions to be possible. The work herein aims to further explore the capability of chemical modification of this bacteriophage as well as to provide a framework for future initiatives toward the fabrication of bionanomaterials based on the Pf1 macromolecular building block. Here, the reactive amines were labelled with an activated ester, the NHS ester of 5(6)-carboxytetramethylrhodamine (NHS-TAMRA), and the resulting conjugates analyzed by spectroscopy and mass spectrometry. In further characterizing the potential utility of this particular filamentous bacteriophage as a biomolecular building block, the reaction of Tyr and Asp/Glu residues were also explored in the context of further bioconjugation to small molecule probes (Fig. **1**). Furthermore, the potential application of Pf1 to the fabrication of advanced materials was explored with glutaraldehyde as a protein crosslinking agent and the resulting constructs were analyzed by scanning electron microscopy (SEM) and fluorescence microscopy.

2. MATERIALS AND METHODS

2.1. Purification of M13 Phage

An overnight culture of ER2738 *E. coli* (New England Biolabs, Whitby, ON, Canada) was diluted 1:100 in lysogeny broth (LB) and inoculated at a final concentration of $1x10^6$ pfu mL^{-1} of purified M13KE. The culture was amplified for 5.5 h at 37°C with shaking to aerate. The bacterial cells were pelleted by centrifugation at 4500 x *g* for 10 min at 10°C. The supernatant was retained and 20 mL 2.5 M NaCl containing 20% polyethylene glycol-8000 (PEG) (PEG/NaCl solution) was added per 80 mL of collected supernatant to precipitate phage overnight at 4°C. The precipitated M13 solution was centrifuged at 12000 x *g* for 15 min at 10°C. The resulting pellet was resuspended in 5 mL of phosphate-buffered saline solution (PBS; 10 mM Na_2HPO_4, 1.8 mM KH_2PO_4, 137 mM NaCl, 2.7 mM KCl) at pH 7.4 per 100 mL of precipitated phage solution. PEG/NaCl solution (1 mL per 5 mL of resuspended M13 pellet) was added to the collected phages and left on ice for 1 h. The solution was centrifuged at 12000 x *g* for 15 min at 10°C. The entirety of the recovered M13 was resuspended in 10 mL PBS (per 1L of amplified M13). The resulting pellet was then centrifuged at 12000 x *g* for 5 min to remove insoluble particles. The supernatant was retained.

2.2. Pf1 Phage

Pf1 bacteriophage (protease-free) was purchased from ASLA Biotech (Riga, Latvia; supplier: Cedarlane, Burlington, Ontario, Canada) at a concentration of 50 mg mL^{-1} (~10^{-6} mol Pf1 L^{-1}) as a suspension in 10 mM potassium phosphate buffer (pH 7.6) 2 mM $MgCl_2$ and 0.05% NaN_3. Pf1 was employed without any further purification; when necessary Pf1 was concentrated by PEG precipitation as described above for M13.

2.3. NHS-TAMRA Bioconjugation

Phage reactions were set up assuming 2700 p8 per M13 or 7400 p8 per Pf1. Reactions were set up with either 12.5 μM $p8_{M13}$, or 25 μM $p8_{Pf1}$ with 250 μM NHS-TAMRA (Click Chemistry Tools, Scottsdale, Arizona) in PBS pH 7.9 with 20% dimethyl sulfoxide (DMSO). Reactions were carried out at 23°C. At certain time points, the reactions were quenched by the addition of tris(hydroxymethyl)aminomethane (Tris) pH 7.9 to a final concentration of 30 mM. Reactions were cleaned up by three rounds of PEG precipitation. Briefly, PEG/NaCl solution was added (1 mL per 5 mL reaction) and precipitated on ice for 25 min before centrifugation at 12700 x *g* for 25 min at 23°C. The final product was resuspended in PBS pH 7.4 and quantified using an equation for phage concentration adapted to consider short-wavelength absorbance of TAMRA.

2.4. Quantifying Phage and TAMRA Conjugates

The amount of M13 present was quantified via UV-Vis absorbance spectroscopy using Eq. (1), an approach analogous to that used by other researchers in quantifying dye-labelled phages [50]. N_{bases} is the number of bases in the M13 ssDNA genome (for M13KE, this is 7222 bp). The 6 x 10^{16} coefficient can be derived from the literature extinction coefficient of 3.84 mg^{-1} cm^{-1} mL [51]. Pf1 was also quantified by its absorbance using Eq. (2). The supplier's extinction coefficient of 2.25 mg^{-1} cm^{-1} mL (used as recommended for quantifying Pf1 phage solutions) [52] and the literature value for the mass of assembled Pf1 phage of 3.4 x 10^7 g mol^{-1} were used to determine the molar amount of Pf1 [44]. For

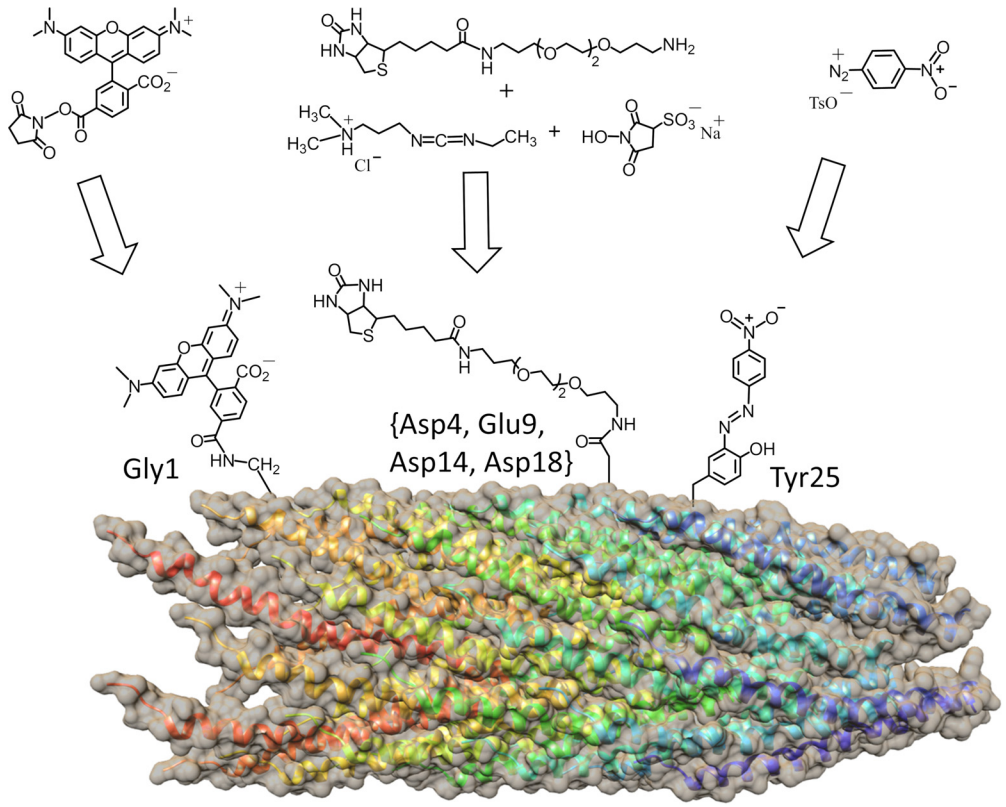

Fig. (1). Bioconjugation strategies employed on the major sheath protein, p8, of Pf1 bacteriophage and include **i**) N-terminal acylation of Gly1 by NHS-TAMRA; **ii**) Asp/Glu coupling to biotin-PEG_3-amine employing EDC/sulfo-NHS activation; **iii**) azo modification of Tyr25 utilizing 4-nitrobenzene diazonium *p*-toluenesulfonate (TsO^-) salt. (*A higher resolution / colour version of this figure is available in the electronic copy of the article*).

Eqs. (1 and 2), a correction factor (CF) of 0.32 (determined from the absorbance at 269/556 nm ratio of the free dye at 43 μM) is included to account for the absorbance of TAMRA when quantifying the TAMRA-conjugated phages. For the unmodified phages, this term was ignored. Furthermore, to account for the light-scattering of phages, the absorbance at 320 nm (A_{320}) was subtracted to avoid overestimating the phage concentration. The dye was also absorbed at this wavelength, and therefore an additional correction factor (CF_{320}) of 0.097 was also included (determined from the ratio of 320/556 nm absorbance of the free dye at 43 μM).

$$[M13] = ((A_{269} - A_{TAMRA,max} \times CF - (A_{320} - CF_{320}\ A_{TAMRA,max})) \times 6 \times 10^{16}) / N_{bases} \quad (1)$$

$$[Pf1] = (A_{270} - A_{TAMRA,max} \times CF - (A_{320} - CF_{320}\ A_{TAMRA,max})) / (2.25 \times MW_{Pf1}) \quad (2)$$

To determine the extent of labelling, the number of p8 subunits per phage was estimated assuming 2700 $p8_{M13}$ for M13 and 7400 $p8_{Pf1}$ for Pf1. The percent labelling was measured using Eq. (3), where $A_{TAMRA,max}$ measures the absorbance at 517 nm for M13 conjugates and 518 nm for Pf1 conjugates. The extinction coefficient of the dye, ε_{TAMRA}, was 65000 M^{-1} cm^{-1} [53].

$$\% \text{ eff.} = ((A_{TAMRA,max} - A_{590})) / (\varepsilon_{TAMRA} \times [pVIII]) \times 100\% \quad (3)$$

To further confirm that this treatment was appropriate for estimating the extent of labelling, the Lowry assay was done alongside a spectrophotometric estimate of Pf1-TAMRA and the resulting estimates were comparable (Suppl. Fig. **1**).

2.5. Other Bioconjugation Reactions

A modification of the strategy reported for tyrosine labeling of the MS2 virus was employed [54]. Preparation of the 4-nitrobenzenediazonium *p*-toluenesulfonate salt was accomplished by the addition of 10 μL of a *p*-nitroaniline solution (20 mg mL^{-1} in CH_3CN) to 5 μL of a *p*-toluenesulfonic acid monohydrate solution (160 mg mL^{-1} in doubly-distilled water (ddH_2O)) at 4°C. A chilled aqueous solution of sodium nitrite (5 μL; 32 mg mL^{-1} in ddH_2O) was then added, and the resulting mixture was left to react for 1 h at 4°C with occasional swirling. The diazonium reagent (6 μL) was then added to a 4°C solution of Pf1 phage (10 μL of a 50 mg mL^{-1} Pf1 solution dissolved in 1 mL of 150 mM potassium phosphate buffer (pH 9.0) providing a final Pf1 concentration of 0.5 mg mL^{-1}). This would correspond to 111 μM $p8_{Pf1}$ subunits with a 15-fold excess of diazonium to $p8_{Pf1}$ subunits. The mixture was then allowed to react at 4°C for 2 h with occasional swirling. The labeled Pf1 was purified by transferring to a 12400 molecular weight cut-off (MWCO) cut-off dialysis tubing and diluting 200-fold into PBS buffer (pH 7.4) for 12 h. The dialysis was conducted twice more to remove low molecular weight molecules.

The Asp/Glu modification was adapted from the carbodiimide bioconjugation method used by Li *et al.* for M13

[49]. Pf1 stock (50 mg mL^{-1}) was first diluted to 5 mg mL^{-1} and dialyzed against concentrated phosphate buffer (cPB; 100 mM Na_2HPO_4, 18 mM KH_2PO_4, 137 mM NaCl, 2.7 mM KCl) pH 7.4 to further purify the Pf1 before the reaction. Pf1 was reacted at a final concentration corresponding to 222 μM p8 subunits with 43 mM *N*-hydroxysulfosuccinimide (sulfo-NHS; 194 eq; Toronto Research Chemicals, North York, Canada), 43 mM biotin-PEG_3-amine (194 eq; Quanta BioDesign, Ltd., Plain City, USA), and 13 mM 1-ethyl-3-(3-dimethylaminopropyl)carbodiimide hydrochloride (EDC; 59 eq; Millipore Sigma, Etobicoke, Canada) in cPB pH 7.4 for 18 h at 23°C. The reaction was cleaned up as described for the Tyr modification using dialysis.

2.6. Mass Spectrometry

Intact phage samples for mass spectrometry (MS) were exchanged into Milli-Q H_2O (MQH_2O) using an Amicon® 10 kilodalton (kDa) MWCO column (Millipore Sigma, Etobicoke, Canada) and then further diluted in 1:1 MeOH:H_2O 0.1% formic acid to a final concentration of 1 μM $p8_{Pf1}$ (8.16 x 10^{10} particles mL^{-1} for Pf1), or 0.5-1 μM $p8_{M13}$ (2.23 x 10^{11} particles mL^{-1}) for analysis. Note, at higher concentrations, M13 were found to precipitate out of solution when diluted into 1:1 MeOH:H_2O 0.1% formic acid and was first diluted to ~5 μM p8 subunits in water before subsequent dilution into MS solvents. Mass spectra were collected on a Thermo Scientific Q-Exactive Orbitrap equipped with an electrospray ionization (ESI) source. The raw mass spectra were deconvoluted using BioPharma Finder™ (ThermoScientific, v.3.0).

Tandem mass spectrometry (MS-MS) spectra were obtained on a Thermo Scientific Q-Exactive Orbitrap equipped with an ESI source. The normalized collisional energy (NCE) on the instrument was set to 30. MS-MS spectra were fit to anticipated fragments from the known sequence of $p8_{Pf1}$ using mMass open source software (version 5.5.0) [55]. Additional details can be found in the figure legends of the relevant supplemental figures.

2.7. Transmission Electron Microscopy

Phage samples were deposited onto carbon/formvar coated 400 mesh copper grids (Ted Pella, Redding, California) at a particle concentration of 3x10^{11} pfu mL^{-1} for 1 min. Grids were briefly washed twice in MQH_2O, and then stained for 20 sec with 1% phosphotungstic acid (neutral, in MQH_2O). For Pf1, after adhering to the phage, the grid was incubated with 0.1% bovine serum albumin (BSA) in Tris-buffered saline solution (TBS; 50 mM Tris, 150 mM NaCl, pH 7.5) for 10 min. Excess BSA was blotted off and the grid was washed three times with TBS, and then three times with MQH_2O before staining. The BSA was used to improve the uniformity of the staining. M13 phages were imaged at 60 kV using a CM10 Philips microscope modified with an Advanced Microscopy Techniques image capturing CCD camera.

2.8. Pf1 Biomaterial Fabrication

Pf1 (2.5 mg; 50 mg mL^{-1}) was further concentrated using PEG/NaCl solution followed by centrifugation as above. The pellet was resuspended to a final volume of 15 μL. After pipetting un-crosslinked Pf1 onto glass slides (2.5 mg), 10 μL of 20% glutaraldehyde was added without mixing and crosslinking carried out 1 day at 23°C. For composite Pf1 biomaterials, Pf1-TAMRA was included at 3.8% by mass.

2.9. Scanning Electron Microscopy

Pf1 biomaterial samples were fixed to standard SEM stubs with carbon tape and sputter-coated with ~10 nm thick gold film to improve sample conduction. The samples were imaged on a Zeiss Ultra Plus field emission SEM with an electron beam energy of 10 keV. Unmodified Pf1 at an initial solution concentration of 50 mg mL^{-1} was air-dried onto a clean silicon chip before the gold-sputtering coating and imaging as described above.

2.10. Confocal Fluorescence Microscopy

Pf1 biomaterials were crosslinked directly onto glass slides and imaged on a Zeiss LSM 510 Meta Confocal Microscope. Briefly, 250 μg Pf1 with 3.7 μg Pf1-TAMRA was mixed and air-dried on a slide for 1 h. For crosslinking, 10 μL of 20% glutaraldehyde was added for 1 h prior to washing the slide with MQH_2O. Excitation of the sample was done with a HeNe1 laser line (543 nm) with NFT 545 filter to pass wavelengths of 545 nm and longer to the detector. The sample was retained after microscopy and store in MQH_2O at 23°C.

2.11. Molecular Modeling

The biological unit of Pf1 from the Protein Data Bank (PDB: 1QL1) [56] was downloaded (ww.rcsb.org) [57]. This structure contained 35 p8 subunits providing 1610 residues (46 residues/subunit). The protein preparation wizard protocol was employed in Maestro (Schrödinger Release 2019-1: Maestro, Schrödinger, LLC, New York, NY, 2019) [58]. The downloaded structure was preprocessed which included the assignment of bond orders, the addition of hydrogen atoms, missing side chains and loops were added using the program Prime (which added the N-terminal Gly1 residue whose coordinates are not provided in the PDB file), and residue charges were generated using the program Epik (pH 7.0 +/- 2.0) [59, 60]. Following this preprocessing stage, the structure was refined which included hydrogen bond assignments and optimization, and a restrained minimization to converge heavy atoms to a root mean square deviation (RMSD) of 0.3 Å employing the OPLS3e forcefield (OPLS3e, Schrödinger, Inc., New York, NY, 2013) [61]. The prepared phage structure had no detected problems with any part of the minimized structure such as steric clashes or high energy bond lengths, bond angles, or dihedral angles.

NHS-TAMRA was modeled in its 5-carboxylate form. Its structure was drawn in Maestro and geometry minimized using the OPLS3e forcefield in MacroModel (Schrödinger Release 2019-1: MacroModel, Schrödinger, LLC, New York, NY, 2019). Subsequently, a conformational search conducted in water was performed using a mixed torsional/Low-mode sampling protocol (default settings were utilized for other variables). Conformers less than 21 kJ/mol above the lowest energy structure were kept. The lowest en-

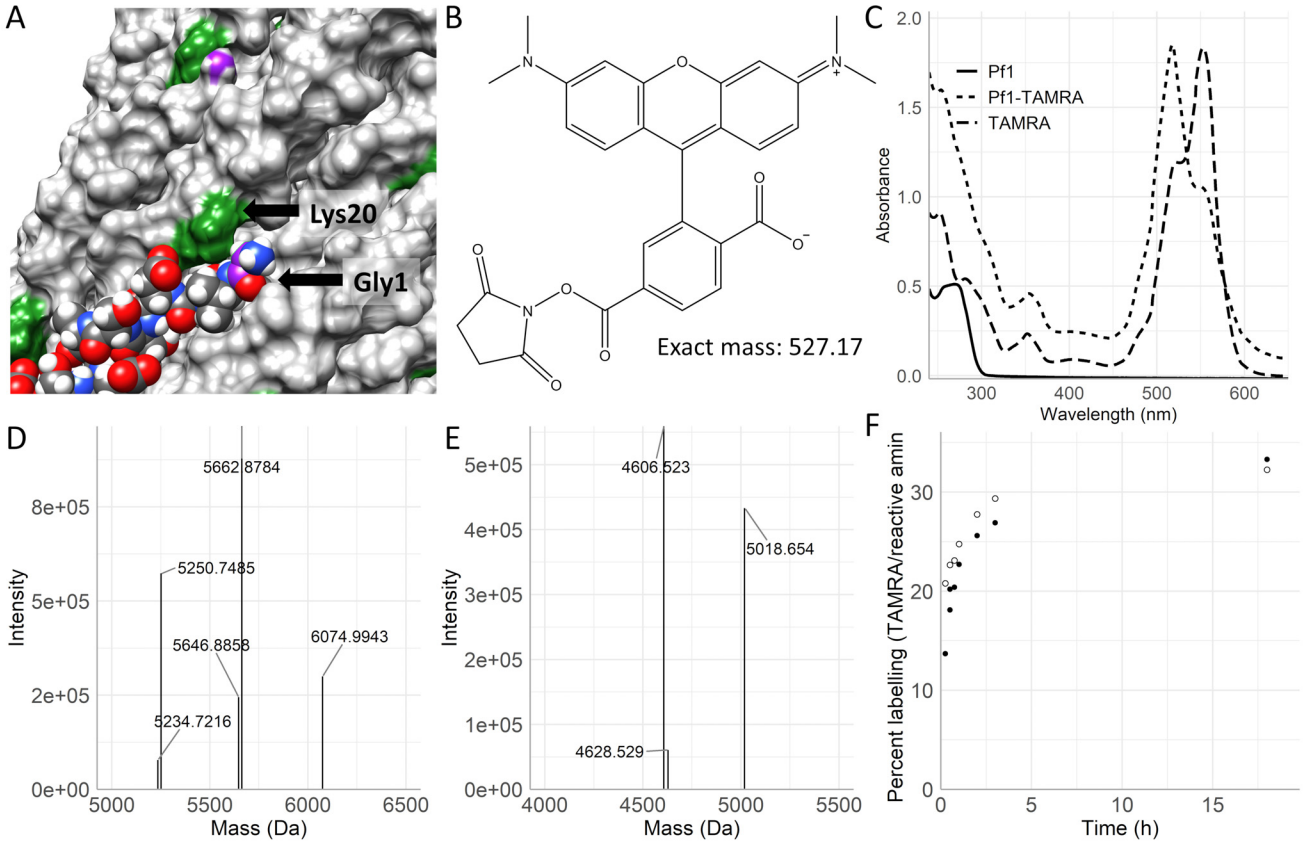

Fig. (2). TAMRA-labelling of Ff phages M13 and Pf1. **A**) Pf1 major coat protein (PDB:1QL1 [50]). Lys20 (green) and Gly1 (purple) on two separate subunits indicated with arrows. **B**) Structure of TAMRA with mass and expected fragment mass of aminolysis adduct. **C**) Individual component spectra of Pf1 (0.7 mg mL^{-1}), NHS-TAMRA (110 μM) and Pf1-TAMRA (estimated 0.7 mg mL^{-1} Pf1 total, and 110 μM p8-TAMRA). **D**) Deconvoluted ESI-MS of M13 (120 μM p8) reacted with 1 mm NHS-TAMRA. **E**) Deconvoluted ESI-MS of Pf1 (120 μM $p8_{Pf1}$) reacted with 1 mM NHS-TAMRA. **F**) Time course of percent labelling of major coat proteins of Pf1 (25 μM $p8_{Pf1}$ subunits; black circles) and M13 (12.5 μM $p8_{M13}$ subunits; open circles) reacted with 250 μM NHS-TAMRA. (*A higher resolution / colour version of this figure is available in the electronic copy of the article*).

ergy structure found in this way was then used as the structure represented in the main text.

3. RESULTS AND DISCUSSION

3.1. NHS-TAMRA Labelling

Several bioconjugation reactions were used to probe the susceptibility of various residues to chemical modification (Fig. **1**). In order to further explore Pf1 coat protein modification with future bionanomaterial fabrication in mind, initial bioconjugation using a fluorescent probe was employed. Relative positions of the N-terminal Gly and Lys20 are shown in Fig. (**2A**). NHS-TAMRA (Fig. **2B**), an amine-reactive dye which absorbs maximally at 554 nm was reacted in 10-fold excess with Pf1 bacteriophage at an amount equivalent to 25 μM $p8_{Pf1}$ to determine labeling efficiencies. The absorbance spectrum of the Pf1-TAMRA conjugate was compared to the spectra of equivalent amounts of the individual components, Pf1 and NHS-TAMRA, showing good agreement (Fig. **2C**).

The reaction of NHS-TAMRA to Pf1 blue-shifts the absorbance maximum from 554 to 518 nm consistent with the formation of parallel dye (H-dimer) aggregates, an observation previously noted for small, well-defined organic scaffolds containing adjacent fluorescent dyes [62-64]. The repetitive structure and close packing of $p8_{Pf1}$ subunits probably contribute to the very drastic shift, resulting in a very high 518/554 ratio of ~1.8, as the TAMRA moieties are expected to be in very similar chemical environments. This value is somewhat higher than covalent TAMRA dimers linked by a relatively short 1,2-diaminoethane linker (519/550=1.5) [63], though lower than a similar TAMRA dimer with a slightly longer linker allowing for more interaction (520/554=2.64) [62]. As the value here falls between these values, it is possible that there are at least two populations of TAMRA on the surface of Pf1: TAMRA without any neighbors to dimerize with and TAMRA where two neighboring $p8_{Pf1}$ subunits are labelled. This is consistent with similar observations on the fluorescence of labelled M13 upon high fluorophore labeling [49]. In contrast, under lower percent labelling conditions where only a single TAMRA molecule per p8 occurs on M13, this blue-shift in the absorbance spectrum is absent, likely due to greater separation of dye constrained to the viral coat [47].

The Pf1-TAMRA conjugate was compared to M13-TAMRA conjugates by mass spectrometry for further comparison. As previously established, at high concentrations of NHS-TAMRA, M13 is capable of modification with two NHS-TAMRA per p8 subunit [49]. This is also observed in the present study for M13 at 64% labelling efficiency of TAMRA per p8 (Fig. **2D**). Note that the M13 sample was oxidized as its mass was 16 Da higher than the expected mono-isotopic mass of 5234 Da but the relative delta masses of the mono- and duo-labelled p8 had the expected change of 412.15 Da. In contrast, under these same conditions for Pf1 (71% labelling efficiency of TAMRA per p8) there were protein masses observed only for the unmodified and the mono-labelled Pf1 $p8_{Pf1}$ (Fig. **2E**). The expected monoisotopic mass of unmodified $p8_{Pf1}$ is 4606.5 Da, and the expected mass for TAMRA-labelled $p8_{Pf1}$is 5018.6 Da. Given that both samples had approximately the same extent of TAMRA labelling the results are consistent with only one amine being accessible to react with NHS-TAMRA on $p8_{Pf1}$.

Furthermore, on-line fragmentation (MS-MS) on the Pf1-TAMRA peak indicated the presence of TAMRA reacted to N-terminal fragments of $p8_{Pf1}$ (Suppl. Figs. **2** and **3**). A fragment containing Lys20 and not the N-terminus could not be positively identified, and therefore Lys20 modification cannot be absolutely discounted; however, it is clear that the N-terminus is labelled by this treatment. Labelling at the N-terminal Gly1 is more likely given its accessibility and lower expected pKa [65]. Additionally, in M13 the N-terminus is preferentially modified and labelled Lys8 occurs only in the presence of higher concentrations of NHS-TAMRA [49]. In previous work characterizing $p8_{Pf1}$ reactivity using succinic anhydride, labeling results lead to the conclusion that the N-terminus and, to a lesser extent, Lys20 were accessible [48]. Furthermore, the inspection of recent fiber diffraction data of Pf1 (PDB: 1QL1) indicated that the N-terminal Gly1 is in close proximity to Lys20 (Fig. **2A**) [56]. Labelling at Gly1 might be expected to further hinder the acylation of a second NHS-TAMRA at the Lys20 of the adjacent subunit (Fig. **3**). It is possible that given the relatively larger size of NHS-TAMRA compared to succinic anhydride that modification of Lys20 is more hindered with this particular activated ester.

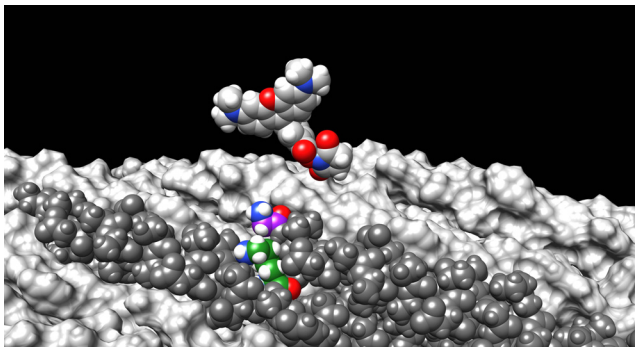

Fig. (3). NHS-TAMRA model adjacent to Gly1 (purple) and Lys20 (green) on Pf1 surface (PDB: 1QL1 [50]). The structure is based on PDB 1QL1 with N-terminal Gly1 built as described in Methods. (*A higher resolution / colour version of this figure is available in the electronic copy of the article*).

The reaction rates of NHS-TAMRA with either M13 or Pf1 were qualitatively compared at 23°C. The extents of reaction for M13 and Pf1 were monitored by estimating phage-conjugated TAMRA produced as described in the methods (Fig. **2F**). At 3 h, the reactions reached 27 and 29% labelling efficiency (dye/reactive amine) for Pf1 and M13, with final values of 33 and 32% showing very similar rates of product formation despite there being twice as many p8 subunits in the Pf1 reaction than the M13 reaction. Since the mass spectrometry analysis indicated that $p8_{Pf1}$ is labelled only once, this result is consistent as the reactions would therefore have had an equal number of reactive amines (Fig. **2E**). In combination with the MS-MS results of NHS-TAMRA labelled Pf1, this would seem to indicate a single reactive amine on $p8_{Pf1}$ for activated esters such as the dye used here. Per subunit, M13 is expected to be more densely labelled than Pf1 which could contribute to the tendency of M13 labelled to a high degree with NHS-TAMRA to aggregate in solution. Overall, a difference in the reactivity profiles of M13 and Pf1 with activated esters is observed.

3.2. Pf1 Tyr and Glu/Asp Reactions

To further characterize the reactivity of Pf1 to bioconjugation reactions, modification of Tyr and Glu/Asp residues was explored (Fig. **1**). The Tyr labelling protocol, employing 4-nitrodiazonium *p*-toluenesulfonate, was based on that of Hooker *et al.* [54, 66]. In their work, the resulting azo-labeled Tyr residue was further converted into an *o*-amino Tyr derivative which could be further reacted with a dienophile via a hetero Diels-Alder reaction to afford more complex bioconjugates. To test the feasibility of this type of modification with Pf1, the filamentous phage was reacted to form the Tyr azo intermediate which was detected by mass spectrometry (Fig. **4A**). The mass at 4755.5 Da corresponds to the mass of the $p8_{Pf1}$ major coat protein with the expected azo adduct. Given the hinderance expected at Tyr40 the only possible location of the modification is at Tyr25 which is expected to be more exposed to solvent.

The Glu/Asp modification was carried out via carbodiimide coupling, similar to that described on M13 by Li *et al*. [49], but employing a biotin-PEG_3-amine to react with the activated carboxyl groups. The success of adduct formation was determined by MS initially and then further confirmed by detection and estimation of the extent of biotinylation by a fluorescence assay using the fluorescent biotin analogue, biotin-4-fluorescein (B4F). The expected adduct mass was detected by MS at 5034.73 Da (Fig. **4B**). Given the difficulty with quantitating the extent of modification by MS, the biotin analogue biotin-4-fluorescein (B4F), was used to create a fluorescence standard curve to which modified Pf1-biotin was assessed in a competitive binding assay with streptavidin (SA). Using this method, the extent of biotinylation was estimated to be ~10.7 ± 1.1 % biotin/p8, or approximately 792 ± 81 biotin/Pf1 (Suppl. Fig. **4**). In Pf1 there are four potential carboxyl groups at which modification might occur: Asp4, Asp14, Asp18, and Glu9. The exact location of the modification was not determined due to the low ionization of the modified p8 subunit. However, where lower levels of modification are required, this is a viable strategy. It is therefore conceivable that these additional modifications, which have been used in other phage bioconjugation

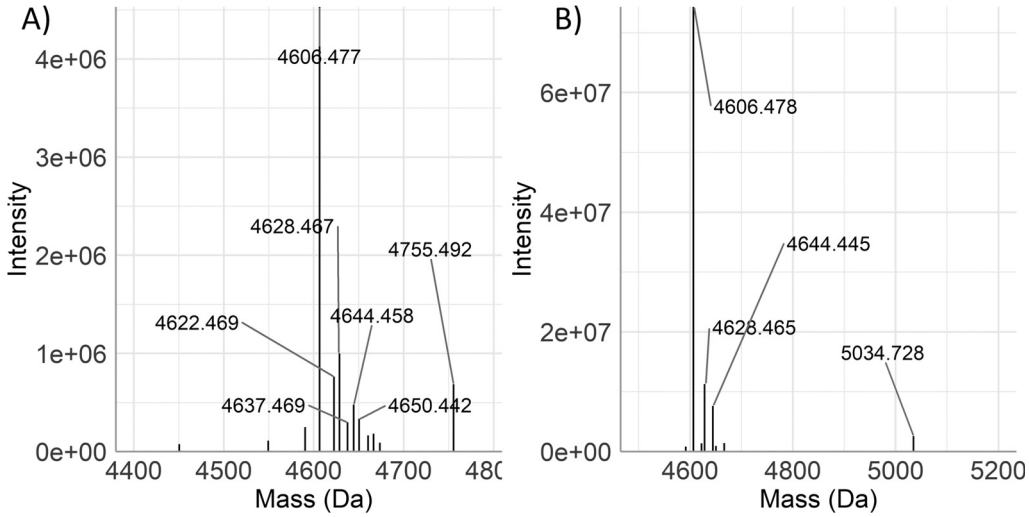

Fig. (4). Mass spectra of additional bioconjugation reactions. **A**) Deconvoluted ESI-MS showing diazotization of Tyr on $p8_{Pf1}$ major coat protein. **B**) Deconvoluted ESI-MS showing carbodiimide coupling of carboxyl groups on $p8_{Pf1}$. (*A higher resolution / colour version of this figure is available in the electronic copy of the article*).

strategies, might also be used with Pf1 for applications where modification with different components are required.

3.3. Pf1/Pf1-TAMRA Crosslinking

M13 has been a critical component in the development of various advanced materials [37-40]. The capability of crosslinking Pf1 for the possibility of preparing functional materials was explored in the current investigation. Preparing crosslinked biomaterials from a filamentous phage with potentially 7400 points of attachment permits the possibility to prepare additional functionalization that might not be possible with crosslinking of smaller, globular proteins. Transmission electron microscopy (TEM) images of the starting materials, un-modified Pf1 and Pf1-TAMRA, were captured (Fig. **5A** and **5B**). These images show the expected filamentous structure to remain after TAMRA bioconjugation and the imaged phages are consistent with the expected diameter of 5.3-6.3 nm [44]. Pf1-TAMRA tended to aggregate on the TEM grid surface, though the filamentous structure was preserved. The black spots in the micrograph are likely artifacts from uneven staining with heavy metal stain.

Initially, dimethyl adipimate (DMA) and glutaraldehyde were used separately as crosslinkers with concentrated Pf1. Biomembranes formed using up to 0.5 M DMA formed a soft hydrogel which fragmented when attempting to manipulate (not shown). Glutaraldehyde instead produced crosslinked materials sturdy enough to be handled with tweezers (Fig. **6A**). Pf1-TAMRA was mixed with Pf1 and crosslinked with glutaraldehyde employing an identical strategy (Fig. **6B**). The material produced utilized Pf1 as the bulk component with 3.8% Pf1-TAMRA by mass. The resulting biomembrane was pink in color and physically handled similarly to the Pf1-only crosslinked material.

The glutaraldehyde crosslinked biomaterials were examined by SEM to determine whether there were notable surface features (Fig. **6D** and **6E**). At a magnification of 30000x little porosity or distinguishing surface features were evident for either the Pf1 or the Pf1/Pf1-TAMRA crosslinked biomaterials. The lack of pores or any kind of filamentous feature observable under these conditions is possibly due to the predictable high density (estimated by the dimensions of the crosslinked materials and total mass of Pf1 used to prepare them) of 400-500 mg Pf1 cm^{-3} present in the samples. It is possible that the slow evaporation of water and subsequent shrinkage as the samples dried compressed any surface features. Shrinkage and damage to the sample due to evaporation is a known issue with preparing biomaterials for SEM [67]. Pure Pf1 (50 mg mL^{-1}) was air-dried onto silicon and also examined by SEM without any crosslinking (Fig. **6F**). In support of the idea that lack of surface features or pores is due to densely packed Pf1, the resulting surface was also featureless, however a few fractures had formed in the surface where the underlying structure of the membrane could be seen. The strands visible by SEM are larger than individual Pf1 and are likely bundles of phage which appear randomly oriented and woven together. Overall, the materials produced using this method are very dense. In the case where more controlled methods of phage deposition are employed, such as by using layer-by-layer deposition, as has been done for M13, one can observe nanoscale features [40]. Also, methods where the biomaterial is fabricated at lower densities of filamentous phage (M13), can result in observable nanodimensional fine structure [39]. While crosslinking of Pf1 does produce a stable material, further refinement of the fabrication process will need to be optimized for a specific use, such as those that might function as membranes.

3.4. TAMRA Fluorescence in Crosslinked Material

The initial Pf1/Pf1-TAMRA fabricated biomaterial was examined using fluorescence microscopy to confirm the presence and detect the localization, of the Pf1-TAMRA bacteriophage in the crosslinked composite. It was apparent that Pf1-TAMRA was indeed present in the biomaterial but heterogeneously blended with the unlabeled Pf1 as observed by the apparent pockets of detected fluorescence (Fig. **6C**). Given the hydrophobic nature of TAMRA, it is possible that the Pf1-TAMRA aggregates form microscopic pockets of

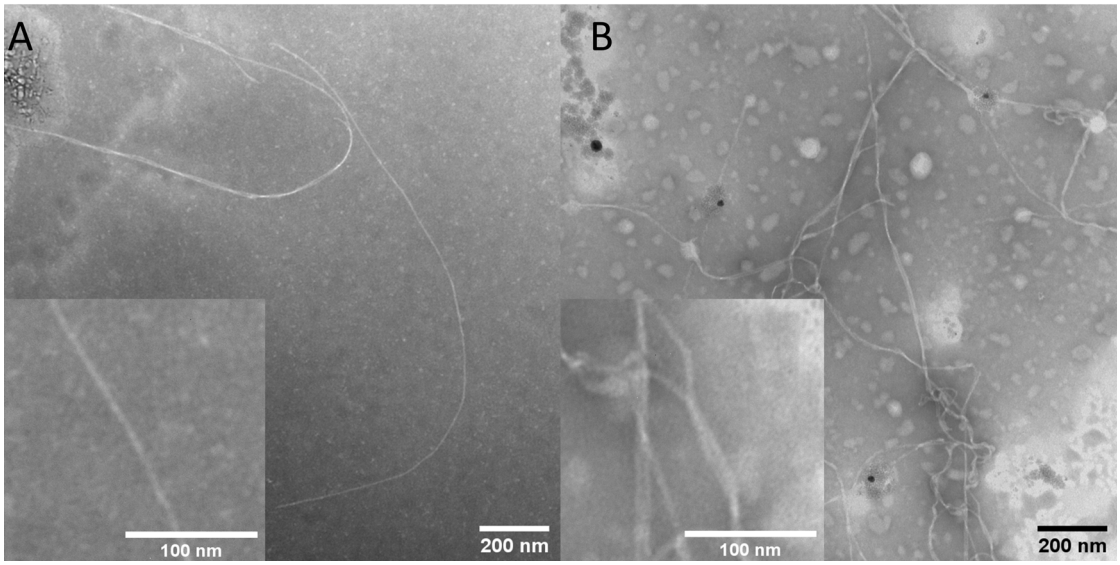

Fig. (5). TEM analysis of starting materials for producing Pf1 biomaterial. **A**) TEM micrograph of Pf1. **B**) TEM micrograph of PF1 labelled with NHS-TAMRA. (*A higher resolution / colour version of this figure is available in the electronic copy of the article*).

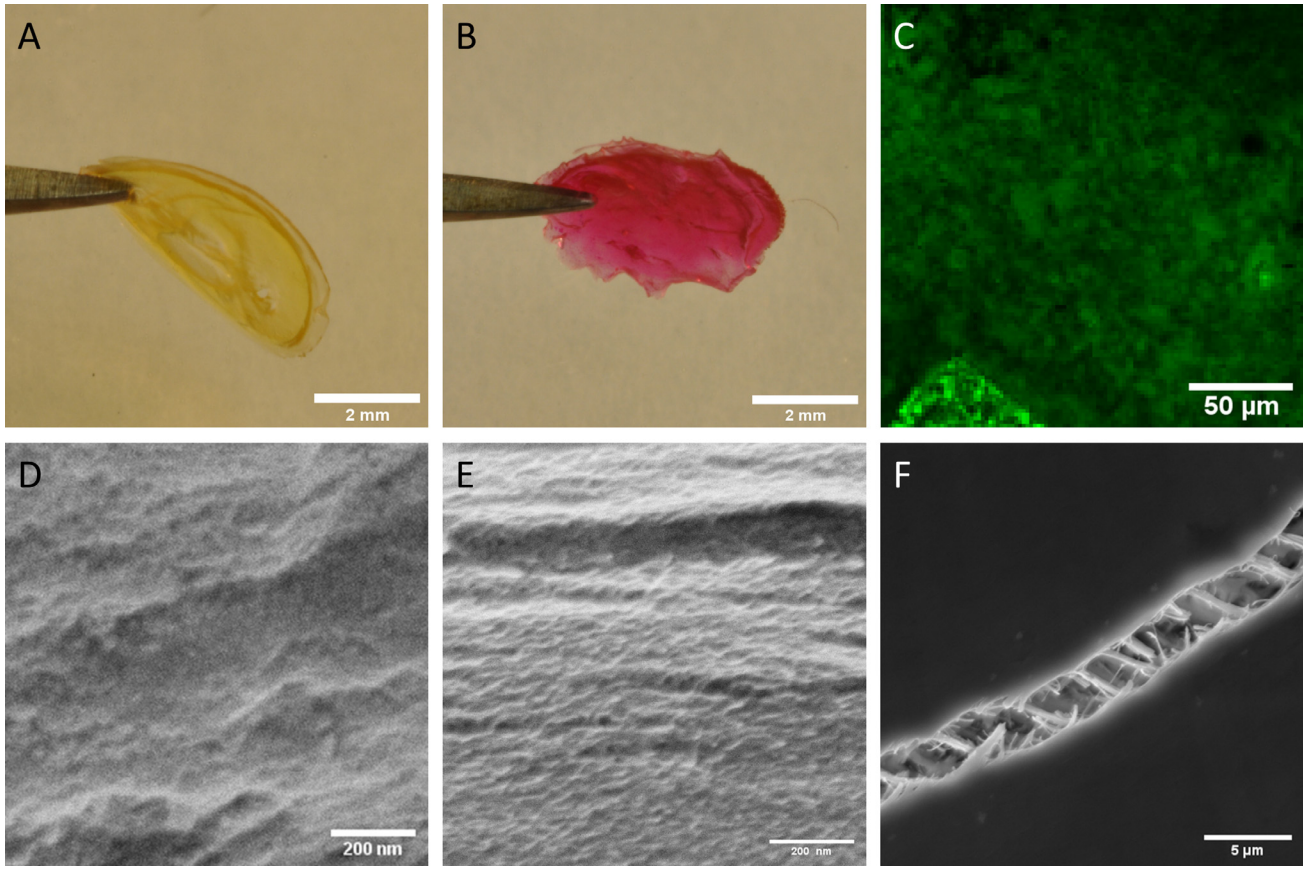

Fig. (6). Pf1-based biomaterials formed by crosslinking with 50% glutaraldehyde. **A**) Glutaraldehyde crosslinked Pf1. **B**) Glutaraldehyde crosslinked Pf1/Pf1-TAMRA. **C**) Confocal microscopy image with 543 nm excitation and NFT 545 emission filters of crosslinked Pf1/Pf1-TAMRA in b). **D**) SEM image of crosslinked Pf1 crosslinked in a). **E**) SEM of crosslinked Pf1/Pf1-TAMRA in b). **F**) SEM micrograph of concentrated Pf1 (50 mg mL^{-1}; un-crosslinked) dried on silicon overnight followed by SEM. The portion imaged shows a crack in an otherwise featureless surface. (*A higher resolution / colour version of this figure is available in the electronic copy of the article*).

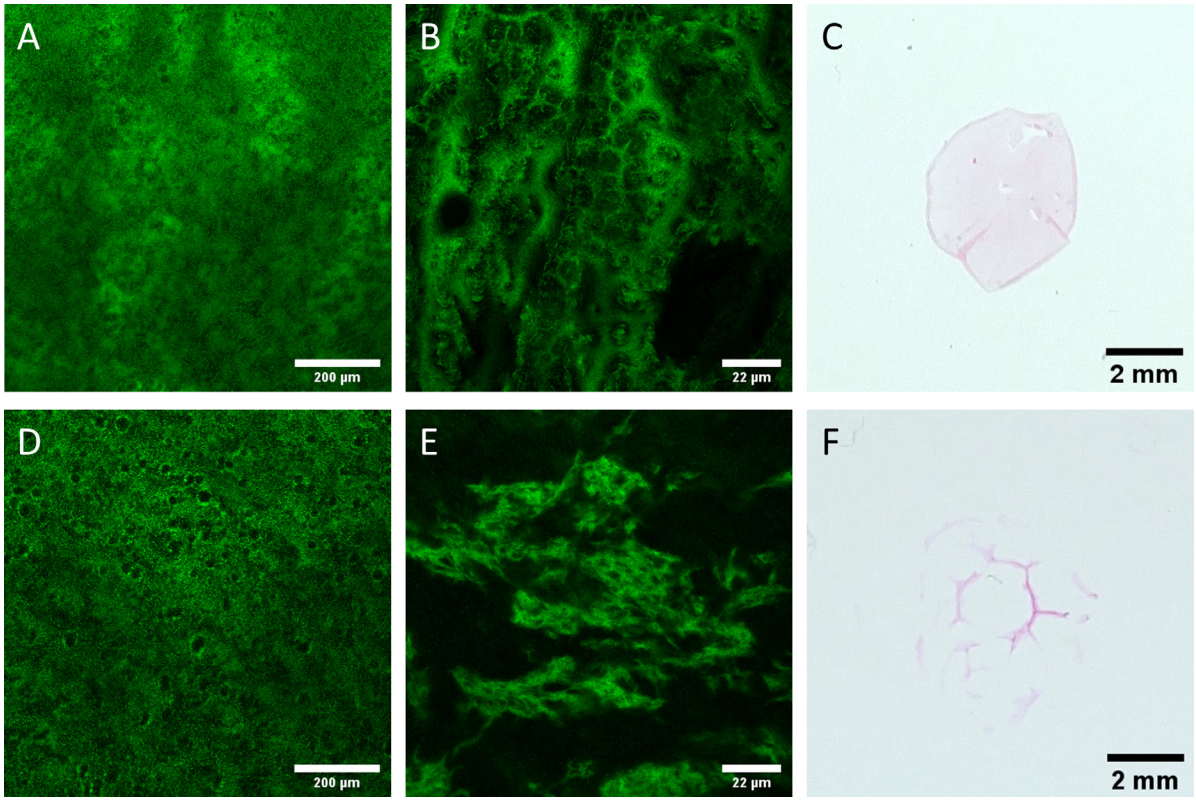

Fig. (7). Confocal microscopy of Pf1/Pf1-TAMRA composite (543 nm excitation and NFT 545 emission filters). **A**) Low magnification (10x objective lens) image of Pf1/Pf1-TAMRA crosslinked with glutaraldehyde 1h, **B**) and under high magnification (63x objective lens). **C**) Crosslinked Pf1/Pf1-TAMRA recovered after imaging. **D**-**F**) Same settings as a-b) except Pf1/Pf1-TAMRA was imaged without any crosslinking. F) Without crosslinker the material is disrupted on removal of coverslip. (*A higher resolution / colour version of this figure is available in the electronic copy of the article*).

functionality within the biomaterial. Given the resolution and magnification limits for the confocal microscopy images, one cannot comment on the integrity of the individual Pf1 phages, as their length (2 µm) [44] is too small to determine this. However, filamentous phages have been applied to crosslinking applications to produce materials where the phage was shown to be intact and it is presumed the phage is also intact here [68-73]. Additional fluorescence characterization was carried out on Pf1/Pf1-TAMRA crosslinked directly on a glass slide alongside the same blend of Pf1/Pf1-TAMRA without crosslinker. At low magnification, functionalized Pf1-TAMRA was observed to be distributed throughout the material (Fig. **7A**). At higher magnification, it becomes apparent that functionalized Pf1-TAMRA is distributed throughout the bulk biomaterial in patches or clusters (Fig. **7B**).

The appearance of these clusters was different between the crosslinked and non-crosslinked blend. When crosslinked by glutaraldehyde the construct appeared more like a network of functionalization, while the Pf1-TAMRA gathered in loosely connected "islands" in the absence of crosslinker (Fig. **7D** and **7E**). Lastly, the crosslinked material was collected from the slide after microscopic observation and could be manipulated with tweezers (though quite delicate due to the thinness of the membrane), while the Pf1/Pf1-TAMRA without crosslinker was smeared upon removing the coverslip (Fig. **7C** and **7F**). Indeed, the total time that this biomaterial was crosslinked was only 1 hour before excess glutaraldehyde was washed off, unlike the initial construct which was crosslinked for over 24 hours. The crosslinked material could be immersed in water for at least 70 days while remaining intact and without any apparent leeching of Pf1-TAMRA. This indicates that Pf1-TAMRA is able to form part of the crosslinked network having several amines already reacted to TAMRA or is otherwise trapped in the material. The fluorescence characterization indicates aggregation of Pf1-TAMRA within the biomaterial. It is likely that reacting different functional groups to the coat protein, in particular, more water-soluble moieties than the TAMRA fluorophore, could result in the fabrication of more homogenous material with functional components.

A very recent appreciation that there are substantially more phages than previously believed to exist underscores the critical need to explore the bioconjugation chemistry of phage in order to exploit this vast reservoir of macromolecular biopolymers for future bionanomaterial fabrication [74]. The present study provides a critical evaluation of the Pf1 bacteriophage's capability for bioconjugation and the modified Pf1's ability for subsequent crosslinking to fabricate solid bionanomaterials. Future work will focus on more elaborate modifications followed by con-

trolled crosslinking strategies or "grafting from" polymerization [75] studies, enabling synthesis of more advanced nanodimensional architectures. Due to a large number of modifiable functional groups on each Pf1 building block, applications of Pf1-based membranes can be extended to sophisticated conducting nanocomposites by incorporation of conductive additives such as carbon nanotubes and polyaniline [68], into tissue engineering scaffolds and smart bandages [17-19], and employed in the fabrication of nanoporous filtration biofilms [40].

CONCLUSION

Based on the current investigation, Pf1can be readily and uniquely modified by NHS-TAMRA at the N-terminal Gly1 of its major sheath protein, p8. In addition, Glu/Asp as well as Tyr residues on the p8 protein can be bioconjugated employing carbodiimide or diazotization chemistries, respectively. A biocomposite of wild type and TAMRA-functionalized Pf1 phage can be fabricated into a bulk material by glutaraldehyde crosslinking.

ETHICS APPROVAL AND CONSENT TO PARTICIPATE

Not applicable.

HUMAN AND ANIMAL RIGHTS

No Animals/Humans were used for studies that are the basis of this research.

CONSENT FOR PUBLICATION

Not applicable.

AVAILABILITY OF DATA AND MATERIALS

The authors confirm that the data supporting the findings of this study are available within the article.

FUNDING

The authors would like to thank NSERC (Canada) for Discovery grants (JH, KTL), NSERC (Canada) for a PGS-D (TU), and NSERC USRA (BH).

CONFLICT OF INTEREST

The authors declare no conflict of interest, financial or otherwise.

ACKNOWLEDGEMENTS

The authors wish to thank Mishi Groh for their expertise in confocal microscopy imaging.

SUPPLEMENTARY MATERIAL

Supplemental Material includes additional details on TAMRA/biotin labelling, MS-MS data of Pf1-TAMRA and SDS-PAGE of Pf1-TAMRA.

REFERENCES

[1] Molek, P.; Bratkovič, T. Bacteriophages as scaffolds for bipartite display: designing swiss army knives on a nanoscale. *Bioconjug. Chem.,* **2015**, *26*(3), 367-378. http://dx.doi.org/10.1021/acs.bioconjchem.5b00034 PMID: 25654261

[2] Petrescu, D.S.; Blum, A.S. Viral-based nanomaterials for plasmonic and photonic materials and devices. *Wiley Interdiscip. Rev. Nanomed. Nanobiotechnol.,* **2018**, *10*(4), e1508. http://dx.doi.org/10.1002/wnan.1508 PMID: 29418076

[3] He, D.; Marles-Wright, J. Ferritin family proteins and their use in bionanotechnology. *N. Biotechnol.,* **2015**, *32*(6), 651-657. http://dx.doi.org/10.1016/j.nbt.2014.12.006 PMID: 25573765

[4] Lee, E.J. Recent advances in protein-based nanoparticles. *Korean J. Chem. Eng.,* **2018**, *35*, 1765-1778. http://dx.doi.org/10.1007/s11814-018-0102-0

[5] Malam, Y.; Loizidou, M.; Seifalian, A.M. Liposomes and nanoparticles: nanosized vehicles for drug delivery in cancer. *Trends Pharmacol. Sci.,* **2009**, *30*(11), 592-599. http://dx.doi.org/10.1016/j.tips.2009.08.004 PMID: 19837467

[6] Barile, L.; Vassalli, G. Exosomes: Therapy delivery tools and biomarkers of diseases. *Pharmacol. Ther.,* **2017**, *174*, 63-78. http://dx.doi.org/10.1016/j.pharmthera.2017.02.020 PMID: 28202367

[7] Chidchob, P.; Sleiman, H.F. Recent advances in DNA nanotechnology. *Curr. Opin. Chem. Biol.,* **2018**, *46*, 63-70. http://dx.doi.org/10.1016/j.cbpa.2018.04.012 PMID: 29751162

[8] Chen, W.; Yu, H.; Lee, S.-Y.; Wei, T.; Li, J.; Fan, Z. Nanocellulose: a promising nanomaterial for advanced electrochemical energy storage. *Chem. Soc. Rev.,* **2018**, *47*(8), 2837-2872. http://dx.doi.org/10.1039/C7CS00790F PMID: 29561005

[9] Chen, Z.; Li, N.; Li, S.; Dharmarwardana, M.; Schlimme, A.; Gassensmith, J.J. Viral chemistry: the chemical functionalization of viral architectures to create new technology. *Wiley Interdiscip. Rev. Nanomed. Nanobiotechnol.,* **2016**, *8*(4), 512-534. http://dx.doi.org/10.1002/wnan.1379 PMID: 26663821

[10] Pokorski, J.K.; Steinmetz, N.F. The art of engineering viral nanoparticles. *Mol. Pharm.,* **2011**, *8*(1), 29-43. http://dx.doi.org/10.1021/mp100225y PMID: 21047140

[11] Wang, Q.; Lin, T.; Tang, L.; Johnson, J.E.; Finn, M.G. Icosahedral virus particles as addressable nanoscale building blocks. *Angew. Chem. Int. Ed. Engl.,* **2002**, *41*(3), 459-462. http://dx.doi.org/10.1002/1521-3773(20020201)41:3<459::AID-ANIE459>3.0.CO;2-O PMID: 12491378

[12] Pokorski, J.K.; Breitenkamp, K.; Liepold, L.O.; Qazi, S.; Finn, M.G. Functional virus-based polymer-protein nanoparticles by atom transfer radical polymerization. *J. Am. Chem. Soc.,* **2011**, *133*(24), 9242-9245. http://dx.doi.org/10.1021/ja203286n PMID: 21627118

[13] Sen Gupta, S.; Kuzelka, J.; Singh, P.; Lewis, W.G.; Manchester, M.; Finn, M.G. Accelerated bioorthogonal conjugation: a practical method for the ligation of diverse functional molecules to a polyvalent virus scaffold. *Bioconjug. Chem.,* **2005**, *16*(6), 1572-1579. http://dx.doi.org/10.1021/bc0501471 PMID: 16287257

[14] Li, S.; Dharmarwardana, M.; Welch, R.P.; Ren, Y.; Thompson, C.M.; Smaldone, R.A.; Gassensmith, J.J. Template-directed synthesis of porous and protective core–shell bionanoparticles. *Angew. Chem. Int. Ed. Engl.,* **2016**, *55*(36), 10691-10696. http://dx.doi.org/10.1002/anie.201604879 PMID: 27485579

[15] Choi, D.S.; Jin, H.-E.; Yoo, S.Y.; Lee, S.-W. Cyclic RGD peptide incorporation on phage major coat proteins for improved internalization by HeLa cells. *Bioconjug. Chem.,* **2014**, *25*(2), 216-223. http://dx.doi.org/10.1021/bc4003234 PMID: 24328047

[16] DePorter, S.M.; McNaughton, B.R. Engineered M13 bacteriophage nanocarriers for intracellular delivery of exogenous proteins to human prostate cancer cells. *Bioconjug. Chem.,* **2014**, *25*(9), 1620-1625. http://dx.doi.org/10.1021/bc500339k PMID: 25134017

[17] Lee, J.Y.; Chung, W-J.; Kim, G. A mechanically improved virus-based hybrid scaffold for bone tissue regeneration. *RSC Advances,* **2016**, *6*, 55022-55032. http://dx.doi.org/10.1039/C6RA07054J

[18] Wang, J.; Yang, M.; Zhu, Y.; Wang, L.; Tomsia, A.P.; Mao, C. Phage nanofibers induce vascularized osteogenesis in 3D printed bone scaffolds. *Adv. Mater.,* **2014**, *26*(29), 4961-4966. http://dx.doi.org/10.1002/adma.201400154 PMID: 24711251

[19] Lee, H.-S.; Kang, J.-I.; Chung, W.-J.; Lee, D.H.; Lee, B.Y.; Lee, S.-W.; Yoo, S.Y. Engineered phage matrix stiffness-modulating

osteogenic differentiation. *ACS Appl. Mater. Interfaces,* **2018**, *10*(5), 4349-4358. http://dx.doi.org/10.1021/acsami.7b17871 PMID: 29345898

[20] Mao, C.; Solis, D.J.; Reiss, B.D.; Kottmann, S.T.; Sweeney, R.Y.; Hayhurst, A.; Georgiou, G.; Iverson, B.; Belcher, A.M. Virus-based toolkit for the directed synthesis of magnetic and semiconducting nanowires. *Science,* **2004**, *303*(5655), 213-217. http://dx.doi.org/10.1126/science.1092740 PMID: 14716009

[21] Park, J.P.; Do, M.; Jin, H-E.; Lee, S-W.; Lee, H. M13 bacteriophage displaying DOPA on surfaces: fabrication of various nanostructured inorganic materials without time-consuming screening processes. *ACS Appl. Mater. Interfaces,* **2014**, *6*(21), 18653-18660. http://dx.doi.org/10.1021/am506873g PMID: 25317741

[22] Zaman, M.S.; Haberer, E.D. Mineralization and optical characterization of copper oxide nanoparticles using a high aspect ratio biotemplate. *J. Appl. Phys.,* **2014**, *116,* 154308. http://dx.doi.org/10.1063/1.4898809

[23] Moradi, M.; Kim, J.C.; Qi, J.; Xu, K.; Li, X.; Ceder, G.; Belcher, A.M. A bio-facilitated synthetic route for nano-structured complex electrode materials. *Green Chem.,* **2016**, *18*, 2619-2624. http://dx.doi.org/10.1039/C6GC00273K

[24] De Plano, L.M.; Scibilia, S.; Rizzo, M.G.; Crea, S.; Franco, D.; Mezzasalma, A.M.; Guglielmino, S.P.P. One-step production of phage-silicon nanoparticles by PLAL as fluorescent nanoprobes for cell identification. *Appl. Phys., A Mater. Sci. Process.,* **2018**, *124*, 222. http://dx.doi.org/10.1007/s00339-018-1637-y

[25] Nam, K.T.; Kim, D.W.; Yoo, P.J.; Chiang, C.Y.; Meethong, N.; Hammond, P.T.; Chiang, Y.M.; Belcher, A.M. Virus-enabled synthesis and assembly of nanowires for lithium ion battery electrodes. *Science,* **2006**, *312*(5775), 885-888. http://dx.doi.org/10.1126/science.1122716 PMID: 16601154

[26] Lee, B.Y.; Zhang, J.; Zueger, C.; Chung, W.-J.; Yoo, S.Y.; Wang, E.; Meyer, J.; Ramesh, R.; Lee, S.-W. Virus-based piezoelectric energy generation. *Nat. Nanotechnol.,* **2012**, *7*(6), 351-356. http://dx.doi.org/10.1038/nnano.2012.69 PMID: 22581406

[27] Chen, P-Y.; Dang, X.; Klug, M.T.; Qi, J.; Dorval Courchesne, N-M.; Burpo, F.J.; Fang, N.; Hammond, P.T.; Belcher, A.M. Versatile three-dimensional virus-based template for dye-sensitized solar cells with improved electron transport and light harvesting. *ACS Nano,* **2013**, *7*(8), 6563-6574. http://dx.doi.org/10.1021/nn4014164 PMID: 23808626

[28] Jeong, C.K.; Kim, I.; Park, K.-I.; Oh, M.H.; Paik, H.; Hwang, G.-T.; No, K.; Nam, Y.S.; Lee, K.J. Virus-directed design of a flexible $BaTiO_3$ nanogenerator. *ACS Nano,* **2013**, *7*(12), 11016-11025. http://dx.doi.org/10.1021/nn404659d PMID: 24229091

[29] Shin, D.-M.; Han, H.J.; Kim, W.-G.; Kim, E.; Kim, C.; Hong, S.W.; Kim, H.K.; Oh, J.-W.; Hwang, Y.-H. Bioinspired piezoelectric nanogenerators based on vertically aligned phage nanopillars. *Energy Environ. Sci.,* **2015**, *8*, 3198-3203. http://dx.doi.org/10.1039/C5EE02611C

[30] Lee, H.-E.; Lee, H.K.; Chang, H.; Ahn, H.-Y.; Erdene, N.; Lee, H.-Y.; Lee, Y.-S.; Jeong, D.H.; Chung, J.; Nam, K.T. Virus templated gold nanocube chain for SERS nanoprobe. *Small,* **2014**, *10*(15), 3007-3011. http://dx.doi.org/10.1002/smll.201400527 PMID: 24700483

[31] Oh, J.-W.; Chung, W.-J.; Heo, K.; Jin, H.-E.; Lee, B.Y.; Wang, E.; Zueger, C.; Wong, W.; Meyer, J.; Kim, C.; Lee, S.-Y.; Kim, W.-G.; Zemla, M.; Auer, M.; Hexemer, A.; Lee, S.-W. Biomimetic virus-based colourimetric sensors. *Nat. Commun.,* **2014**, *5*, 3043. http://dx.doi.org/10.1038/ncomms4043 PMID: 24448217

[32] Adhikari, M.; Strych, U.; Kim, J.; Goux, H.; Dhamane, S.; Poongavanam, M-V.; Hagström, A.E.V.; Kourentzi, K.; Conrad, J.C.; Willson, R.C. Aptamer-phage reporters for ultrasensitive lateral flow assays. *Anal. Chem.,* **2015**, *87*(23), 11660-11665. http://dx.doi.org/10.1021/acs.analchem.5b00702 PMID: 26456715

[33] Brasino, M.; Lee, J.H.; Cha, J.N. Creating highly amplified enzyme-linked immunosorbent assay signals from genetically engineered bacteriophage. *Anal. Biochem.,* **2015**, *470*, 7-13. http://dx.doi.org/10.1016/j.ab.2014.10.006 PMID: 25447463

[34] Yan, Y.; Zhang, M.; Moon, C.H.; Su, H.-C.; Myung, N.V.; Haberer, E.D. Viral-templated gold/polypyrrole nanopeapods for an ammonia gas sensor. *Nanotechnology,* **2016**, *27*(32), 325502. http://dx.doi.org/10.1088/0957-4484/27/32/325502 PMID: 27354441

[35] Lee, J.H.; Fan, B.; Samdin, T.D.; Monteiro, D.A.; Desai, M.S.; Scheideler, O.; Jin, H.-E.; Kim, S.; Lee, S.-W. Phage-based structural color sensors and their pattern recognition sensing system. *ACS Nano,* **2017**, *11*(4), 3632-3641. http://dx.doi.org/10.1021/acsnano.6b07942 PMID: 28355060

[36] Koh, E.H.; Mun, C.; Kim, C.; Park, S.-G.; Choi, E.J.; Kim, S.H.; Dang, J.; Choo, J.; Oh, J.-W.; Kim, D.-H.; Jung, H.S. M13 bacteriophage/silver nanowire surface-enhanced raman scattering sensor for sensitive and selective pesticide detection. *ACS Appl. Mater. Interfaces,* **2018**, *10*(12), 10388-10397. http://dx.doi.org/10.1021/acsami.8b01470 PMID: 29505228

[37] Niu, Z.; Bruckman, M.A.; Harp, B.; Mello, C.M.; Wang, Q. Bacteriophage M13 as a scaffold for preparing conductive polymeric composite fibers. *Nano Res.,* **2008**, *1*, 235-241. http://dx.doi.org/10.1007/s12274-008-8027-2

[38] Courchesne, N.-M.D.; Klug, M.T.; Chen, P.-Y.; Kooi, S.E.; Yun, D.S.; Hong, N.; Fang, N.X.; Belcher, A.M.; Hammond, P.T. Assembly of a bacteriophage-based template for the organization of materials into nanoporous networks. *Adv. Mater.,* **2014**, *26*(21), 3398-3404. http://dx.doi.org/10.1002/adma.201305928 PMID: 24648015

[39] Jung, S.M.; Qi, J.; Oh, D.; Belcher, A.; Kong, J. M13 virus aerogels as a scaffold for functional inorganic materials. *Adv. Funct. Mater.,* **2017**, *27,* 1603203. http://dx.doi.org/10.1002/adfm.201603203

[40] Devaraj, V.; Han, J.; Kim, C.; Kang, Y.-C.; Oh, J.-W. Self-assembled nanoporous biofilms from functionalized nanofibrous M13 bacteriophage. *Viruses,* **2018**, *10*(6), 322. http://dx.doi.org/10.3390/v10060322 PMID: 29895757

[41] Hansen, M.R.; Mueller, L.; Pardi, A. Tunable alignment of macromolecules by filamentous phage yields dipolar coupling interactions. *Nat. Struct. Biol.,* **1998**, *5*(12), 1065-1074. http://dx.doi.org/10.1038/4176 PMID: 9846877

[42] Hennig, J.; Militti, C.; Popowicz, G.M.; Wang, I.; Sonntag, M.; Geerlof, A.; Gabel, F.; Gebauer, F.; Sattler, M. Structural basis for the assembly of the Sxl-Unr translation regulatory complex. *Nature,* **2014**, *515*(7526), 287-290. http://dx.doi.org/10.1038/nature13693 PMID: 25209665

[43] Marvin, D.A.; Symmons, M.F.; Straus, S.K. Structure and assembly of filamentous bacteriophages. *Prog. Biophys. Mol. Biol.,* **2014**, *114*(2), 80-122. http://dx.doi.org/10.1016/j.pbiomolbio.2014.02.003 PMID: 24582831

[44] Day, L.A.; Marzec, C.J.; Reisberg, S.A.; Casadevall, A. DNA packing in filamentous bacteriophages. *Annu. Rev. Biophys. Biophys. Chem.,* **1988**, *17*, 509-539. http://dx.doi.org/10.1146/annurev.bb.17.060188.002453 PMID: 3293598

[45] Mohan, K.; Weiss, G.A. Chemically modifying viruses for diverse applications. *ACS Chem. Biol.,* **2016**, *11*(5), 1167-1179. http://dx.doi.org/10.1021/acschembio.6b00060 PMID: 26930417

[46] Pires, D.P.; Cleto, S.; Sillankorva, S.; Azeredo, J.; Lu, T.K. Genetically engineered phages: A review of advances over the last decade. *Microbiol. Mol. Biol. Rev.,* **2016**, *80*(3), 523-543. http://dx.doi.org/10.1128/MMBR.00069-15 PMID: 27250768

[47] Urquhart, T.; Daub, E.; Honek, J.F. Bioorthogonal modification of the major sheath protein of bacteriophage M13: extending the versatility of bionanomaterial scaffolds. *Bioconjug. Chem.,* **2016**, *27*(10), 2276-2280. http://dx.doi.org/10.1021/acs.bioconjchem.6b00460 PMID: 27626459

[48] Nakashima, Y.; Konigsberg, W.H. Chemical modification and molecular orientation of the B protein in the filamentous bacterial virus Pf1. *J. Mol. Biol.,* **1980**, *138*(3), 493-501. http://dx.doi.org/10.1016/S0022-2836(80)80014-3 PMID: 6774098

[49] Li, K.; Chen, Y.; Li, S.; Nguyen, H.G.; Niu, Z.; You, S.; Mello, C.M.; Lu, X.; Wang, Q. Chemical modification of M13 bacteriophage and its application in cancer cell imaging. *Bioconjug. Chem.,* **2010**, *21*(7), 1369-1377. http://dx.doi.org/10.1021/bc900405q PMID: 20499838

[50] Zhang, Z.; Grelet, E. Tuning chirality in the self-assembly of rod-like viruses by chemical surface modifications. *Soft Matter.,* **2013**, *9*, 1015-1024. http://dx.doi.org/10.1039/C2SM27264D

[51] Berkowitz, S.A.; Day, L.A. Mass, length, composition and structure of the filamentous bacterial virus fd. *J. Mol. Biol.,* **1976**, *102*(3), 531-547. http://dx.doi.org/10.1016/0022-2836(76)90332-6 PMID: 775110

[52] Fleming, K.; Matthews, S. Media for Studies of Partially Aligned States. In: *Protein NMR Techniques;*; Downing, A.K., Ed.; *Methods in Molecular BiologyTM; Humana Press:*; Downing, A.K., Ed.; Totowa, NJ, **2004**. http://dx.doi.org/10.1385/1-59259-809-9:079

[53] Meadows, D.L.; Shafer, J.S.; Schultz, J.S. Determining the extent of labeling for tetramethylrhodamine protein conjugates. *J. Immunol. Methods,* **1991**, *143*(2), 263-272. http://dx.doi.org/10.1016/0022-1759(91)90051-G PMID: 1719100

[54] Hooker, J.M.; Kovacs, E.W.; Francis, M.B. Interior surface modification of bacteriophage MS2. *J. Am. Chem. Soc.,* **2004**, *126*(12), 3718-3719. http://dx.doi.org/10.1021/ja031790q PMID: 15038717

[55] Strohalm, M.; Kavan, D.; Novák, P.; Volný, M.; Havlícek, V. mMass 3: a cross-platform software environment for precise analysis of mass spectrometric data. *Anal. Chem.,* **2010**, *82*(11), 4648-4651. http://dx.doi.org/10.1021/ac100818g PMID: 20465224

[56] Welsh, L.C.; Symmons, M.F.; Marvin, D.A. The molecular structure and structural transition of the α-helical capsid in filamentous bacteriophage Pf1. *Acta Crystallogr. D Biol. Crystallogr.,* **2000**, *56*(Pt 2), 137-150. http://dx.doi.org/10.1107/S0907444999015334 PMID: 10666593

[57] Berman, H.M.; Westbrook, J.; Feng, Z.; Gilliland, G.; Bhat, T.N.; Weissig, H.; Shindyalov, I.N.; Bourne, P.E. The protein data bank. *Nucleic Acids Res.,* **2000**, *28*(1), 235-242. http://dx.doi.org/10.1093/nar/28.1.235 PMID: 10592235

[58] Sastry, G.M.; Adzhigirey, M.; Day, T.; Annabhimoju, R.; Sherman, W. Protein and ligand preparation: parameters, protocols, and influence on virtual screening enrichments. *J. Comput. Aided Mol. Des.,* **2013**, *27*(3), 221-234. http://dx.doi.org/10.1007/s10822-013-9644-8 PMID: 23579614

[59] Jacobson, M.P.; Pincus, D.L.; Rapp, C.S.; Day, T.J.F.; Honig, B.; Shaw, D.E.; Friesner, R.A. A hierarchical approach to all-atom protein loop prediction. *Proteins,* **2004**, *55*(2), 351-367. http://dx.doi.org/10.1002/prot.10613 PMID: 15048827

[60] Shelley, J.C.; Cholleti, A.; Frye, L.L.; Greenwood, J.R.; Timlin, M.R.; Uchimaya, M. Epik: a software program for pK(a) prediction and protonation state generation for drug-like molecules. *J. Comput. Aided Mol. Des.,* **2007**, *21*(12), 681-691. http://dx.doi.org/10.1007/s10822-007-9133-z PMID: 17899391

[61] Harder, E.; Damm, W.; Maple, J.; Wu, C.; Reboul, M.; Xiang, J.Y.; Wang, L.; Lupyan, D.; Dahlgren, M.K.; Knight, J.L.; Kaus, J.W.; Cerutti, D.S.; Krilov, G.; Jorgensen, W.L.; Abel, R.; Friesner, R.A. OPLS3: A force field providing broad coverage of drug-like small molecules and proteins. *J. Chem. Theory Comput.,* **2016**, *12*(1), 281-296. http://dx.doi.org/10.1021/acs.jctc.5b00864 PMID: 26584231

[62] Christie, R.J.; Tadiello, C.J.; Chamberlain, L.M.; Grainger, D.W. Optical properties and application of a reactive and bioreducible thiol-containing tetramethylrhodamine dimer. *Bioconjug. Chem.,* **2009**, *20*(3), 476-480. http://dx.doi.org/10.1021/bc800367e PMID: 19249862

[63] Hernando, J.; van der Schaaf, M.; van Dijk, E.M.H.P.; Sauer, M.; García-Parajó, M.F.; van Hulst, N.F. Excitonic behavior of rhodamine dimers: A single-molecule study. *J. Phys. Chem. A,* **2003**, *107*, 43-52. http://dx.doi.org/10.1021/jp0218995

[64] Valdes-Aguilera, O.; Neckers, D.C. Aggregation phenomena in xanthene dyes. *Acc. Chem. Res.,* **1989**, *22*, 171-177. http://dx.doi.org/10.1021/ar00161a002

[65] Hermanson, G.T. 1 - Functional Targets. *Bioconjugate Techniques*; Hermanson, G.T., Ed.; Academic Press: San Diego, **1996**, pp. 3-136. http://dx.doi.org/10.1016/B978-012342335-1/50002-6

[66] Schlick, T.L.; Ding, Z.; Kovacs, E.W.; Francis, M.B. Dual-surface modification of the tobacco mosaic virus. *J. Am. Chem. Soc.,* **2005**, *127*(11), 3718-3723. http://dx.doi.org/10.1021/ja046239n PMID: 15771505

[67] Pogorelov, A.G.; Selezneva, I.I. Evaluation of collagen gel microstructure by scanning electron microscopy. *Bull. Exp. Biol. Med.,* **2010**, *150*(1), 153-156. http://dx.doi.org/10.1007/s10517-010-1091-0 PMID: 21161075

[68] Chen, P.-Y.; Hyder, M.N.; Mackanic, D.; Courchesne, N.-M.D.; Qi, J.; Klug, M.T.; Belcher, A.M.; Hammond, P.T. Assembly of viral hydrogels for three-dimensional conducting nanocomposites. *Adv. Mater.,* **2014**, *26*(30), 5101-5107. http://dx.doi.org/10.1002/adma.201400828 PMID: 24782428

[69] Yu, T.; Li, Y.; Yang, T.; Gong, Y.; Sudibya, H.G.; Chen, P.; Luo, K.Q.; Liao, K. Fabrication of all-in-one multifunctional phage liquid crystalline fibers. *RSC Advances,* **2013**, *3*, 20437-20445. http://dx.doi.org/10.1039/c3ra43034k

[70] Mao, J.Y.; Belcher, A.M.; Vliet, K.J.V. Genetically engineered phage fibers and coatings for antibacterial applications. *Adv. Funct. Mater.,* **2010**, *20*, 209-214. http://dx.doi.org/10.1002/adfm.200900782

[71] Chiang, C.-Y.; Mello, C.M.; Gu, J.; Silva, E.C.C.M.; Van Vliet, K.J.; Belcher, A.M. Weaving genetically engineered functionality into mechanically robust virus fibers. *Adv. Mater.,* **2007**, *19*, 826-832. http://dx.doi.org/10.1002/adma.200602262

[72] Niyomdecha, S.; Limbut, W.; Numnuam, A.; Kanatharana, P.; Charlermroj, R.; Karoonuthaisiri, N.; Thavarungkul, P. Phage-based capacitive biosensor for Salmonella detection. *Talanta,* **2018**, *188*, 658-664. http://dx.doi.org/10.1016/j.talanta.2018.06.033 PMID: 30029427

[73] Wu, L.; Lee, L.A.; Niu, Z.; Ghoshroy, S.; Wang, Q. Visualizing cell extracellular matrix (ECM) deposited by cells cultured on aligned bacteriophage M13 thin films. *Langmuir,* **2011**, *27*(15), 9490-9496. http://dx.doi.org/10.1021/la201580v PMID: 21678980

[74] Kuhn, J.H.; Wolf, Y.I.; Krupovic, M.; Zhang, Y.-Z.; Maes, P.; Dolja, V.V.; Koonin, E.V. Classify viruses - the gain is worth the pain. *Nature,* **2019**, *566*(7744), 318-320. http://dx.doi.org/10.1038/d41586-019-00599-8 PMID: 30787460

[75] Willis, B.; Eubanks, L.M.; Wood, M.R.; Janda, K.D.; Dickerson, T.J.; Lerner, R.A. Biologically templated organic polymers with nanoscale order. *Proc. Natl. Acad. Sci. USA,* **2008**, *105*(5), 1416-1419. http://dx.doi.org/10.1073/pnas.0711308105 PMID: 18216240